High Temperature Co-doped $LiMn_2O_4$-Based Spinels. Structural, Electrical, and Electrochemical Characterization

S. Mandal,[†] R. M. Rojas,[†] J. M. Amarilla,[†] P. Calle,[‡] N. V. Kosova,[§] V. F. Anufrienko,[§] and J. M. Rojo*,[†]

Instituto de Ciencia de Materiales de Madrid, Consejo Superior de Investigaciones Cientificas, Cantoblanco, 28049 Madrid, Spain, Departamento de Quimica-Fisica Aplicada, Facultad de Ciencias, UAM, 28049 Madrid, Spain, and Institute of Solid State Chemistry, Russian Academy of Science, 18 Kutateladze, Novosibirsk 630128, Russia

Received August 8, 2001. Revised Manuscript Received January 23, 2002

High-temperature cubic spinels were obtained by thermal treatment at 1100 °C of the corresponding $LiCo_yMn_{2-y}O_4$ ($0 \le y \le 1$) spinels. The samples were characterized by X-ray powder diffraction, thermogravimetric analysis, electron paramagnetic resonance (EPR) spectroscopy, and electrical and electrochemical measurements. The lattice parameter of the new phases in the $0.3 < y \le 1$ range is larger compared to the starting ones. The EPR spectra of the new compounds are also different from the starting ones. The electrical conductivity of the new phases depends on the Co content. For $y > 0.65$ the sharp increase in conductivity observed is associated with a change in electron hopping from Mn^{3+}/Mn^{4+} ions to Co^{2+}/Co^{3+} ones. At high temperatures, the conductivity is explained in terms of phonon-assisted polaron hopping among either Mn^{3+}/Mn^{4+} or Co^{2+}/Co^{3+} nearest neighbors. At low temperatures electron hopping beyond the nearest neighbors accounts for the conductivity. The electrochemical behavior of the new compounds as positive electrodes was analyzed. The discharge curves show both the 4 and 5 V plateau due to the Mn^{4+}/Mn^{3+} and Co^{4+}/Co^{3+} reduction, respectively. Differences in electrochemical characteristics compared to the starting samples are found. From electrochemical and thermogravimetric measurements, the oxidation states of the transition metal ions and the chemical composition of the high-temperature samples are estimated.

Introduction

$LiMn_2O_4$-based materials are among the most extensively studied materials as candidates for cathodes in rechargeable lithium batteries.[1] At room temperature, $LiMn_2O_4$ shows a cubic spinel-type structure, space group $Fd3m$. The structure can be described as ideally consisting of a cubic close-packing arrangement of oxygen ions at the 32e sites, the Li^+ ions occupy the tetrahedral 8a sites, and the Mn^{3+} and Mn^{4+} ions occupy the octahedral 16d sites. The EPR spectrum of $LiMn_2O_4$ shows a very broad signal centered at $g \approx 2$ that has been assigned to paramagnetic Mn^{4+} ions in octahedral sites.[2,3] Thermoelectric power measurements have showed that $LiMn_2O_4$ is an n-type semiconductor, its conductivity being due to electron hopping among Mn^{3+} and Mn^{4+} ions.[4−7] $LiMn_2O_4$ undergoes a reversible cubic ($Fd3m$) ⇔ orthorhombic ($Fddd$) phase transformation at temperatures close to room temperature.[8,9] The phase transition is accompanied by a change in the electrical conductivity, which is lower for the low-temperature orthorhombic phase.[6,10]

In the cubic phase, lithium extraction/insertion from/into the tetrahedral 8a sites occurs at 4 V; it is associated with the $Mn^{3+} \Leftrightarrow Mn^{4+}$ oxidation/reduction process. However, the amount of extracted/inserted lithium decreases gradually on cycling. To prevent it, $LiMn_2O_4$ has been doped by partial substitution for Mn^{3+} by several iso- or aliovalent cations such as Li, Ti, Ge, Fe, Co, Ni, Cr, and Zn.[11−14] Among the cations

* Author for correspondence. E-mail address: jmrojo@icmm.csic.es.
† Consejo Superior de Investigaciones Cientificas.
‡ UAM.
§ Russian Academy of Science.

(1) Tackeray, M. M. *J. Am. Ceram. Soc.* **1999**, *82*, 3347.
(2) Massarotti, V.; Capsoni, D.; Bini, M.; Azzoni, C. B.; Paleari, A. *J. Solid State Chem.* **1997**, *128*, 80.
(3) Stoyanova, R. K.; Zhecheva, E. N.; Gorova, M. Y. *J. Mater. Chem.* **2000**, *10*, 1377.
(4) Goodenough, J. B.; Manthiran, A.; Wnetrzewski, P. *J. Power Sources* **1993**, *43*, 269.
(5) Massarotti, V.; Capsoni, D.; Bini, M.; Chiodelli, G.; Azzoni, C. B.; Mozzati, M. C.; Palleari, A. *J. Solid State Chem.* **1997**, *131*, 94.
(6) Shimakawa, Y.; Numata, T.; Tabuchi, J. *J. Solid State Chem.* **1997**, *131*, 138.
(7) Molenda, J.; Kucza, W. *Solid State Ionics* **1999**, *117*, 41.
(8) Rousse, G.; Masquelier, C.; Rodríguez-Carvajal, J.; Hervieu, M. *Electrochem. Solid-State Lett.* **1999**, *2*, 6.
(9) Rousse, G.; Masquelier, C.; Rodríguez-Carvajal, J.; Elkaim, E.; Lauriat, J. P.; Martínez, J. L. *Chem. Mater.* **1999**, *11*, 3629.
(10) Sugiyama, J.; Atsumi, T.; Koiwai, A.; Sasaki, T.; Hioki, T.; Noda, S.; Kamegashira, N. *J. Phys. (Paris): Condens. Matter* **1997**, *9*, 1729.
(11) Guohua, L.; Ikuta, H.; Uchida, T.; Wakihara, M. *J. Electrochem. Soc.* **1996**, *143*, 178.
(12) Pistoia, G.; Antonini, A.; Rosati, R.; Bellitto, C.; Ingo, G. M. *Chem. Mater.* **1997**, *9*, 1443.
(13) Arora, P.; Popov, B. N.; White, R. E. *J. Electrochem. Soc.* **1998**, *145*, 807.
(14) Strobel, P.; Ibarra Palos, A.; Anne, M.; Le Cras, F. *J. Mater. Chem.* **2000**, *10*, 429.

10.1021/cm011219v CCC: $22.00
Published on Web 03/27/2002

studied, Co seems to be the dopant that yields cathode materials with the highest reversible capacity.[11] Furthermore, it has been recently reported that cubic spinel phases belonging to the $Li_2Co_{1+x}Mn_{3-x}O_8$ ($-1 \le x \le 1$) solid solution can reversibly extract/insert Li^+ ions at voltages of ca. 5 V. It has been associated with the presence of Co^{3+} in the octahedral 16d positions of the spinel structure, and ascribed to the $Co^{3+} \Leftrightarrow Co^{4+}$ oxidation/reduction process.[15,16] The Co-doped samples show an electrical conductivity that depends on the Co content, the conductivity showing a maximum value for the $Li_2CoMn_3O_8$ composition.[16]

When $LiMn_2O_4$ is heated at high temperature, this compound undergoes a weight loss that has been ascribed to oxygen removal. On cooling, oxygen can reversibly show uptake, and under some particular experimental conditions the starting compound is recovered.[17−20] However, quenching from temperatures ≥900 °C seems to prevent that recovering leading to oxygen-deficient samples that show tetragonally distorted spinel structures.[17,20] Thermal studies of $LiMn_2O_4$-doped samples are rather scarce.[21,22] In these samples, oxygen can be removed in an irreversible way, and they transformed into new reduced samples[38] whose electrical and electrochemical properties could be very different from the starting ones.

The aim of this work is to study the new compounds obtained from the thermal treatment of $LiCo_yMn_{2-y}O_4$ ($0 \le y \le 1$) at 1100 °C. The high-temperature samples have been characterized by X-ray powder diffraction and electron paramagnetic resonance spectroscopy. From thermogravimetric analysis the net oxygen loss after the thermal treatment has been determined. The electrochemical response has been analyzed, and the amount of Mn and Co ions in the different oxidation states has been estimated. The electrical conductivity has also been measured and discussed in relation to the chemical composition of the samples. The results obtained in the high-temperature samples are compared with those obtained in the starting samples, which are used as references.

Experimental Section

A series of cobalt-doped spinels with general formula $LiCo_yMn_{2-y}O_4$ ($0 \le y \le 1$) was obtained by reaction between the corresponding mixed cobalt manganese oxide precursors $Co_xMn_{3-x}O_4$ ($0 \le x \le 1.5$) previously synthesized at room temperature, and $LiOH \cdot H_2O$ (Fluka, p.a.). A detailed description of the procedure followed for the synthesis of the $Co_xMn_{3-x}O_4$ precursors was reported elsewhere.[23] Stoichiometric mixtures of $Co_xMn_{3-x}O_4$ and $LiOH \cdot H_2O$ were ground intimately in an agate mortar, fired in air at 450 °C for 3 h and at 750 °C for 24 h. The heating/cooling rates were 2 °C min^{-1}. The samples thus obtained are referred hereafter *as prepared*. Some particular compositions were subjected to an additional thermal treatment at 950 °C for 3 h, followed by annealing at 600 °C for 3 days. The samples thus treated are referred as *annealed*. The series of high-temperature samples was obtained by heating the samples *as prepared* at 1100 °C for 1 h and then cooling to room temperature. The heating/cooling rates were 10 °C min^{-1}. The samples thus treated are referred as *heated* samples. For some particular compositions the lithium content of the *as prepared* and *heated* samples was analyzed by inductively coupled plasma (ICP).

X-ray powder diffraction (XRD) patterns were recorded at room temperature with a Siemens D 501 diffractometer, with Cu Kα radiation. The patterns were scanned in the step-scanning mode at 0.02°(2θ) and 1 s $step^{-1}$ counting time within the range $10° \le 2\theta \le 80°$. Lattice parameters were refined with the CELREF program.[24]

Thermogravimetric (TG) analyses were made on a Stanton STA781 instrument in still air up to 1200 °C, at 10 °C min^{-1} heating/cooling rate. Simultaneous qualitative analysis of the gases evolved during the thermal treatments (EGA) was carried out with a ThermoStar mass spectrometer, with Ar as the gas carrier. Differential scanning calorimetry (DSC) curves were obtained in a Seiko 320U instrument, between −60 and +60 °C in still air and a 10 °C min^{-1} heating/cooling rate.

Electron paramagnetic resonance (EPR) spectra were recorded as the first derivative of the absorption signal, using a Bruker 300E spectrometer, with a 100 kHz field modulation operating at 9.5 GHz frequency. The powder samples were placed in a cylindrical quartz tube of 3 mm inner diameter; the sample weight was 25 mg. The microwave power level was kept at 3 mW. The scan range was 6000 G and the spectra were registered at room temperature. In some particular cases the spectra were also recorded at lower temperatures (−173 and −73 °C).

Electrochemical response was analyzed in a lithium cell. Composites of positive electrodes were prepared from the mentioned samples (≈25 mg or 72 wt %), carbon black (17 wt %), and polyvinylidenefluoride (PVDF, 11 wt %). PVDF was dissolved in *N*-methylpyrrolidone, and the other two components were added to the solution. Then, the solvent was evaporated at 110 °C, and the solid was cold pressed in circular pellets (13 mm diameter). The electrolyte used was a 1 M solution of $LiPF_6$ in ethylene carbonate and dimethyl carbonate as supplied by Merck. The negative electrode was a lithium foil, which also operated as reference electrode. Two-electrode Swagelock cells were assembled within an argon glovebox in which the water content was kept below 1 ppm. The charge and discharge were performed with a potentiostatic/galvanostatic multichannel Arbin instrument by using a constant current of $C/12$, where C is the theoretical capacity of the samples assuming an extraction/insertion of one lithium per formula. The low current used ensured a quasi-equilibrium response. The samples were first oxidized (charge step) up to a $E_{cut-off}$ of 5.4 V to extract lithium; then, they were reduced (discharge step) up to a $E_{cut-off}$ of 3.3V to insert lithium.

Two-probe impedance measurements were carried out in a 1260 Solartron impedance/gain phase analyzer. Circular pellets were made by cold pressing of the *as prepared* samples; then, the pellets were sintered at 1100 °C for 1 h. This treatment is similar to that used for obtaining the *heated* samples, and by this way we have prepared pellets of the *heated* samples in the compositional range $0 \le y \le 1$. A pellet of the *heated* sample at $y = 0.85$ was also subjected to the annealing treatment, and thus transformed into the corresponding *annealed* sample. Silver was used as electrode. The pellets were mounted in an Oxford cryostat, and the temperature was controlled in the range from 150 to −190 °C.

(15) Kawai, H.; Nagata, M.; Tukamoto, H.; West, A. R. *Electrochem. Solid State Lett.* **1998**, *1*, 212.
(16) Kawai, H.; Nagata, M.; Kageyama, H.; Tukamoto, H.; West, A. R. *Electrochim. Acta* **1999**, *45*, 315.
(17) Tarascon, J. M.; McKinnon, W. R.; Coowar, F.; Bowmer, T. N.; Amatucci, G.; Guyomard, D. *J. Electrochem. Soc.* **1994**, *141*, 1421.
(18) Yamada, A.; Miura, K.; Hinokuma, K.; Tanaka, M. *J. Electrochem. Soc.*, **1995**, *142*, 2149.
(19) Tackeray, M. M.; Mansuetto, M. F.; Dees, D. W.; Vissers, D. R. *Mater. Res. Bull.* **1996**, ***31***, 133.
(20) Paulsen, J. M.; Dahn, J. R. *Chem. Mater.* **1999**, *11*, 3065.
(21) Zhong, Q.; Bonakdarpour, A.; Zhang, M.; Gao, Y.; Dahn, J. R. *J. Electrochem. Soc.* **1997**, *144*, 205.
(22) Yamaguchi, R.; Ikuta, H.; Wakihara, M. *J. Therm. Anal. Calorim.* **1999**, *57*, 797.
(23) Amarilla, J. M.; Martín de Vidales, J. L.; Rojas, R. M. *Solid State Ionics* **2000**, *127*, 73.
(24) Laugier, J.; Filhol, A. CELREF. I.L.L. Grenoble, France, unpublished, P.C. Version, 1991.

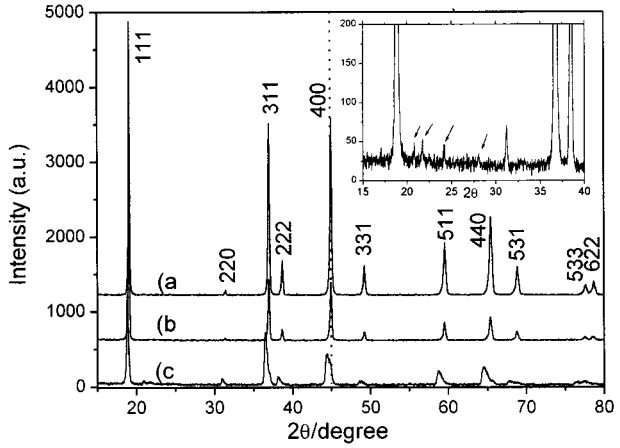

Figure 1. X-ray powder diffraction patterns recorded at room temperature on the Co-doped sample at $y = 0.85$: (a) *as prepared*; (b) *annealed*; (c) *heated*. The inset shows a magnified 2θ region of pattern a. Li_2MnO_3 peaks are marked by arrows.

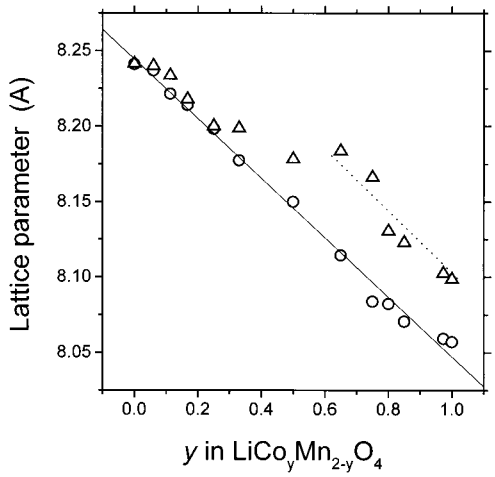

Figure 2. Cubic lattice parameter vs Co content for the *as prepared* (circles) and *heated* (triangles) samples. The solid line is the best linear fit. The dotted line is drawn to guide the eye.

Results

X-ray Powder Diffraction. The X-ray patterns of all samples are similar and they can be indexed using a cubic cell, space group *Fd*3*m*. As an example the patterns recorded for the *as prepared, annealed, and heated* sample at $y = 0.85$ are shown in Figure 1, parts a−c, respectively. A magnification of pattern a between 15 and 40° in 2θ (see the inset) allowed detection of extremely low intensity peaks (arrow marked) that are ascribed to Li_2MnO_3 impurity. In the *annealed* sample (b) the diffraction peaks of the spinel phase appear at the same positions as for the *as prepared* sample (a). However, in the magnified pattern b, the small peaks ascribed to Li_2MnO_3 were not observed (not shown). The pattern of the *heated* sample (c) shows that the diffraction peaks of the spinel phase are broadened and shifted toward lower 2θ angles. In this pattern, the Li_2MnO_3 diffraction peaks are observed as very low intensity peaks.

The lattice parameter of the cubic spinel phase determined for the *as prepared* and *heated* samples is plotted vs Co content (y) in Figure 2. For the *as prepared* samples, the lattice parameter decreases linearly as y increases from 8.2411(7) Å for $y = 0$ to 8.057(2) Å for $y = 1$. For the *heated* samples, the lattice parameter is practically coincident with that of the *as prepared* samples in the $0 \le y \le 0.3$ range. For $y > 0.3$, the *heated* samples show larger lattice parameters compared to the *as prepared* samples. In addition, the lattice parameter of the *heated* samples for $y > 0.65$ decreases linearly, from 8.184(6) Å for $y = 0.65$ to 8.098(5) Å for $y = 1$.

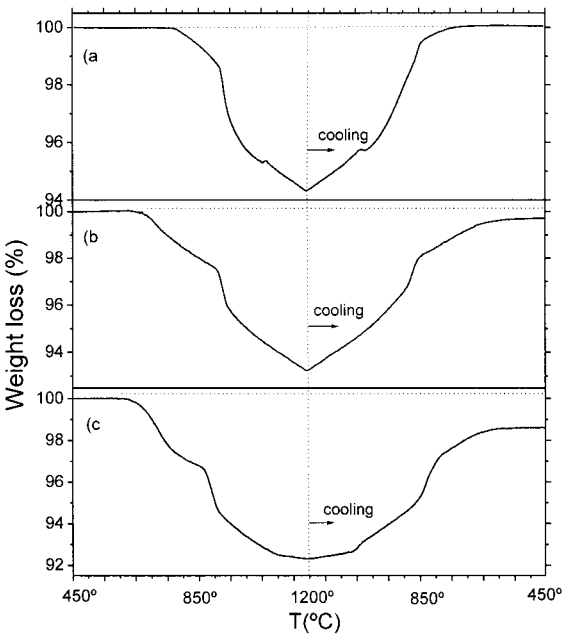

Figure 3. Heating/cooling TG curves for the *as prepared* samples at $y = 0$ (a), 0.5 (b), and 0.85 (c).

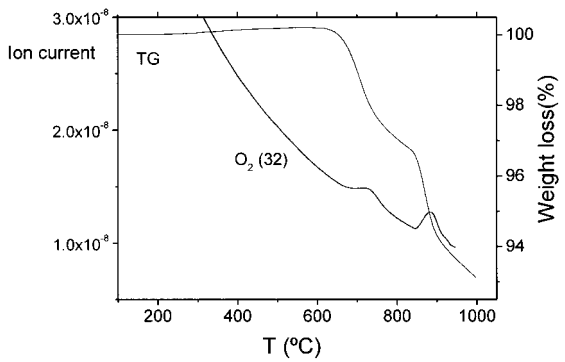

Figure 4. Curves of TG and EG mass spectrometry (O_2) recorded for the *as prepared* sample at $y = 0.75$.

Thermogravimetric Analysis. The TG curves obtained for the *as prepared* samples at $y = 0$, 0.5, and 0.85 are shown in Figure 3,parts a−c, respectively. In the heating run weight is lost, and in the cooling run weight is regained. However, while all the weight is practically regained for samples with $y \le 0.3$, the weight is only partially regained for samples with $y > 0.3$. Gases evolved during the heating run were identified as O_2 (Figure 4). From comparison of the evolved gas curve and the TG curve, both obtained simultaneously on the sample at $y = 0.75$, we can see that the maxima of the oxygen release coincide with the weight losses.

Chemical Analysis. The Li content was determined by ICP on some particular *as prepared* and *heated* samples. As an example the results obtained for the *as prepared* and *heated* sample at $y = 0.75$ were 3.71 and 3.69 wt % of Li, respectively. The theoretical Li content

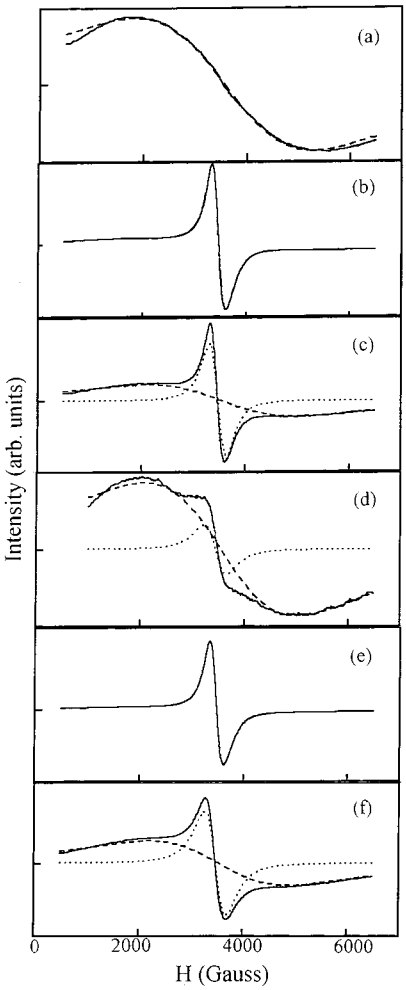

Figure 5. EPR spectra recorded for the *as prepared* samples at $y = 0$ (a), 0.65 (b), 0.85 (c), and 1 (e) and for the *annealed* samples at $y = 0.85$ (d) and 1 (f). Dotted and dashed lines stand for the narrow and broad components, respectively.

is 3.77 wt % for the *as prepared* sample and 3.83 wt % for the *heated* one.

Electron Paramagnetic Resonance. EPR spectra recorded for several *as prepared* and *annealed* samples are shown in Figure 5. The spectrum for the *as prepared* sample at $y = 0$ (a) shows a broad signal centered at $g \approx 2$ that is well fitted to a Lorentzian curve with a peak-to-peak width (ΔH_{pp}) of 348 mT. This signal is similar to that reported by other authors and is assigned to paramagnetic Mn^{4+} ($S = {}^3/_2$) ions interacting with paramagnetic Mn^{4+} and Mn^{3+} ions in the spinel structure.[2,3] The spectra recorded for the *as prepared* samples at $y = 0.65$ (b), 0.85 (c), and 1 (e) show, besides the broad signal, a narrow signal also centered at $g \approx 2$. The latter signal, which shows Lorentzian shape and $\Delta H_{pp} \approx 22$ mT, is identical to that obtained by us (not shown) for pure Li_2MnO_3 and agrees with those reported for Li_2MnO_3.[2,25] The spectra of the *as prepared* samples at $0 < y < 0.65$ (not shown) also displayed the two mentioned signals but their relative intensity changed from sample to sample. The spectra of the *annealed* samples at $y = 0.85$ (d) and 1 (f) show the narrow signal but of lower intensity compared to the corresponding *as prepared* samples. To estimate the amount of the Li_2MnO_3 impurity, mixtures of pure $LiMn_2O_4$ and Li_2MnO_3 were prepared and their EPR spectra recorded.

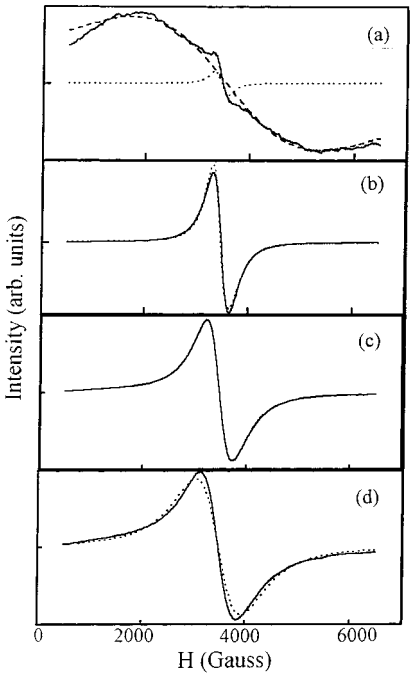

Figure 6. EPR spectra recorded for the *heated* samples at $y = 0$ (a), 0.65 (b), 0.85 (c), and 1 (d). Dotted and dashed lines stand for the components used in the fitting of the spectra.

The EPR spectra recorded on the *heated* samples are shown in Figure 6. For $y = 0$ the spectrum (a) is similar to that of the *as prepared* sample (Figure 5a). However, for the samples at $y = 0.65$ (b), 0.85 (c), and 1 (d) the spectra are different from the corresponding *as prepared* samples (Figure 5, parts b, c, and e). The spectra profile of the *heated* samples prevent us to propose how many signals are required for the fitting. When only one Lorentzian signal is chosen the spectra are ill-reproduced, especially for high Co contents. The ΔH_{pp} of the spectra increases as y increases from 32 mT for $y = 0.65$ to 72 mT for $y = 1$. In all cases the spectra appear centered at $g \approx 2$, and are assigned to Mn^{4+} ions. No signals at $g > 2$ are observed. Some of the spectra were also recorded at lower temperatures (from −173 to −73 °C) but only a slight broadening was observed (not shown).

Electrochemical Characterization. The discharge curves obtained for several *as prepared* samples are shown in Figure 7a. The curve for $y = 0$ ($LiMn_2O_4$) shows the well-known plateau at ca. 4 V due to Mn^{4+}/Mn^{3+} reduction;[26] no electrochemical reaction is observed above 4.5 V. The curves for the Co-doped samples show besides the plateau at ca. 4 V another one at ca. 5 V. The latter plateau has been ascribed to the Co^{4+}/Co^{3+} reduction.[16,27] From the length of each plateau the capacity was determined. We observe that while the capacity at 4 V decreases as y increases, the capacity at 5 V increases. The total discharge capacity seems also to change with y, showing a maximum value of 125 $mAhg^{-1}$ for $y = 0.33$.

The charge and discharge curve for both the *as prepared* and the *heated* sample at $y = 0.5$ are shown

(25) Stoyanova, R.; Gorova, M.; Zhecheva, E. *J. Phys. Chem. Solids* **2000**, *61*, 615.
(26) Guyomard, D.; Tarascon, J. M. *J. Electrochem. Soc.* **1992**, *139*, 937.
(27) Chang, S. H.; Ryu, K. S.; Kim, K. M.; Kim, M. S.; Kim, I. K.; Kang, S. G. *J. Power Sources* **1999**, *84*, 134.

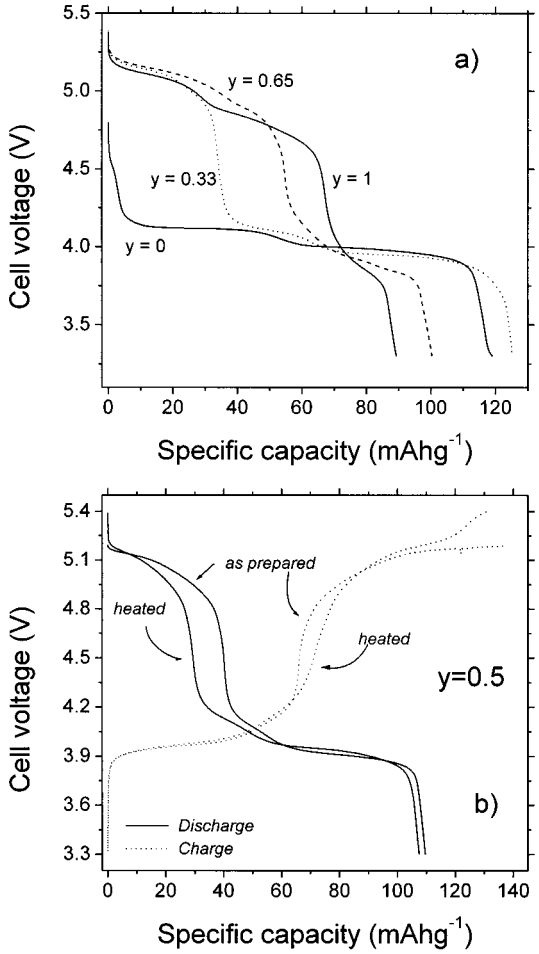

Figure 7. (a) Galvanostatic curves obtained in the first discharge for the *as prepared* samples at $y = 0$, 0.33, 0.65, and 1. (b) Charge (dotted line) and discharge (solid line) curves obtained for the *as prepared* and *heated* samples at $y = 0$. 5.

in Figure 7b. During the charge at high voltage (above 5 V) some degradation of the electrolyte takes place; it explains the higher capacity measured in the charge compared to the discharge. The discharge capacity in the 4 V region is higher for the *heated* sample than for the *as prepared* one. On the contrary, the discharge capacity in the 5 V region is lower for the *heated* sample. Differences in capacity are also found when we compare the two kinds of samples with other Co contents.

Electrical Measurements. Impedance plots recorded at −53 and −113 °C for the *heated* sample at $y = 0.5$ are shown in Figure 8. Two arcs are observed. The experimental data are well-fitted to the equation $Z^* = Z^*_1 + Z^*_2$, where $Z^*_k = 1/(1/R_k + B_k(i\omega)^{nk})$, $k = 1$, 2; i.e., Z^*_1 and Z^*_2 account for a parallel circuit formed of one resistance (parameter R_k) and one universal CPE capacitor (parameters B_k, n_k). So, the total Z^* corresponds to a series arrangement of the two mentioned circuits. The capacitances of the high- and low-frequency arcs (16 pF and 10 nF) allow their ascription to grain interior (or bulk) and grain boundary responses, respectively. From the fittings the resistance associated with each arc is estimated. Then, the dc conductivity of the grain interior response is calculated as usual.[28]

(28) MacDonald, R. J.; Johnson, W. B. In *Impedance Spectroscopy*; MacDonald, R. J., Ed.; John Wiley and Sons: New York, 1987.

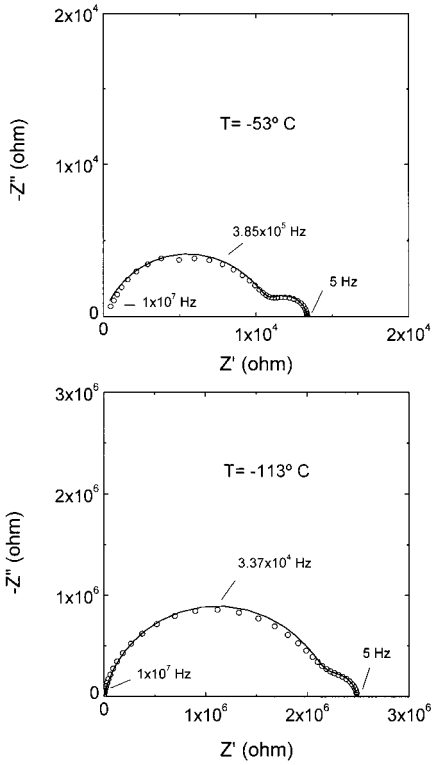

Figure 8. Impedance plots recorded at −53 and at −113 °C for the *heated* sample at $y = 0.5$. Solid lines are the best fits to $Z^* = Z_1^* + Z_2^*$ (for details see text).

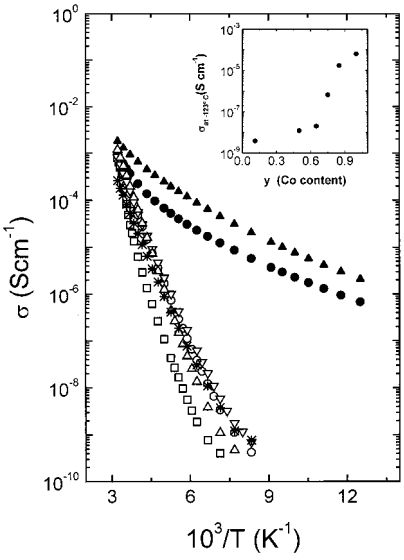

Figure 9. Grain interior dc conductivity (σ) vs reciprocal temperature (1000/T) for the *heated* samples at $y = 0$ (□), 0.11 (△), 0.5 (○), 0.65 (▽), 0.85 (●), and 1 (▲). The conductivity for the *annealed* sample at $y = 0.85$ is also plotted (∗). The variation of the grain interior dc conductivity at −123 °C vs Co content is shown in the inset.

The grain interior dc conductivity (σ) vs reciprocal temperature (1000/T) for several *heated* samples is plotted in Figure 9. Data for the *annealed* sample at $y = 0.85$ (stars in the figure) are also represented. The *heated* sample at $y = 0$ (squares) shows a change in conductivity of approximately 1 order of magnitude, at temperatures close to room temperature, that is associated with the cubic ⇔ orthorhombic phase transition.[6,10] This phase transition gives rise to an exothermic peak

in the DSC curve (not shown). All the other Co-doped samples do not exhibit either the conductivity change or the DSC peak. According to the temperature dependence of the conductivity, the *heated* samples can be grouped in: (i) samples with $y \leq 0.65$, and (ii) samples with $y > 0.65$. The conductivity of the *annealed* sample at $y = 0.85$ is much lower than the corresponding *heated* sample and is close to the conductivity of the *heated* samples at $y \leq 0.65$. The conductivity measured at −123 °C vs y for the *heated* samples is shown in the inset of Figure 9. A sharp increase in conductivity for $y \approx 0.75$ is observed.

Discussion

Structural Characterization. The $LiCo_yMn_{2-y}O_4$ ($0 \leq y \leq 1$) *as prepared* samples show a cubic spinel-type structure. The linear decrease of the lattice parameter as y increases (Figure 2) indicates that the samples belong to a solid solution over the whole compositional range. The lattice parameters found and their variation on doping fairly agree with those reported by several authors,[13,16,29,30] although some departure from the linear dependence has also been reported.[16,30] The shrinkage of the cubic lattice as Co^{3+} replaces Mn^{3+} is explained by the smaller ionic size of Co^{3+} (0.545 Å) compared to Mn^{3+} (0.645 Å).[31] The substitution for Mn^{3+}, which is a paramagnetic ion, by Co^{3+}, which is a diamagnetic one, produces a slight narrowing of the broad Mn^{4+} EPR signal (Figure 5); the peak-to-peak width decreases from ca. 350 mT for $y = 0$ ($LiMn^{3+}Mn^{4+}O_4$) to ca. 260 mT for $y = 1$ ($LiCo^{3+}Mn^{4+}O_4$). A detailed discussion about the dependence of the EPR spectra on temperature and on Co content has been reported elsewhere.[30]

In some particular *as prepared* samples, the cubic spinel phase was accompanied by a Li_2MnO_3 impurity. The X-ray diffraction patterns showed very low intensity peaks that corresponded to Li_2MnO_3 (Figure 1). The EPR spectra showed the narrow signal we assign to Li_2MnO_3 (Figure 5). Our assignment agrees with that reported by some authors[2] and differs from others.[30] From the intensity of the narrow EPR signal we have estimated that the amount of Li_2MnO_3 was in all cases below 1 wt %. Taking this into account, we can consider the *as prepared* samples as being almost pure. The annealing treatment removes the Li_2MnO_3 impurity and does not produce any appreciably variation of the spinel phase as deduced from XRD and EPR data.

When the *as prepared* samples are heated from room temperature to 1100 °C, they undergo a weight loss. Oxygen is removed as deduced from mass spectrometry (Figure 4). On cooling to room temperature the weight is gained. However for some compositions there are a net weight loss (Δw). To ascertain whether Δw is also due to removal of lithium, chemical analysis of lithium was done in some particular *heated* samples. The results of the analyses showed that lithium had not been removed at least in an appreciable amount. The variation of Δw vs y is shown in Figure 10. We observe that

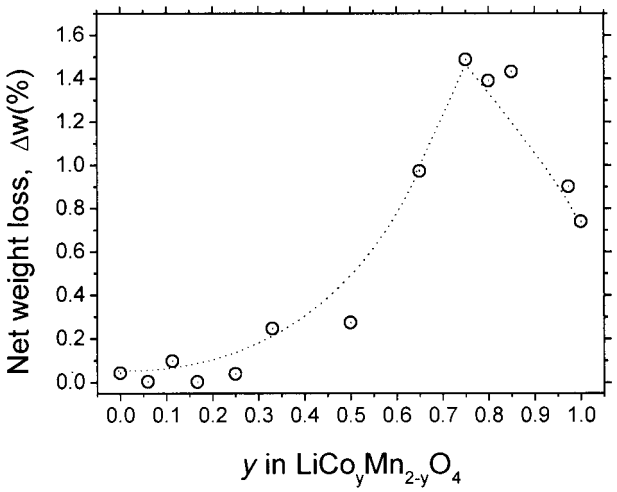

Figure 10. Net weight loss (Δw) vs Co content (y) for the samples after being heated to 1200 °C and cooled to room temperature. The dotted line is a guide to the eye.

$\Delta w \approx 0$ for $y \leq 0.3$, but Δw increases for $y > 0.3$ going through a maximum at $y = 0.75$. Therefore, the $y > 0.3$ *heated* samples are oxygen-deficient samples in which a part of the Co and/or Mn ions could be reduced. These samples also showed cubic spinel structure and in some of them Li_2MnO_3 was segregated as impurity. As the amount of the impurity was very low in all cases, the *heated* samples can be formulated as $LiCo_yMn_{2-y}O_{4-\delta}$ spinels.

The lattice parameter of the *heated* samples for $y \leq 0.3$ (Figure 2) coincides practically with that of the *as prepared* samples, suggesting that both *as prepared* and *heated* are the same. This is also supported by the similar EPR spectra of the *heated* and *as prepared* sample at $y = 0$ (Figures 6a and 5a). For $y > 0.3$, the lattice parameter of the *heated* samples is systematically larger than that of the *as prepared* ones. It can be explained in terms of a reduction of the transition metal ions; i.e., part of the Mn^{4+} is reduced to Mn^{3+} and/or part of the Co^{3+} is reduced to Co^{2+}. As the reduced Mn^{3+} and Co^{2+} have larger ionic radii than Mn^{4+} and Co^{3+}, respectively, their contributions cause the lattice parameter of the spinel structure to increase. The complex EPR spectra observed for the *heated* samples (Figure 6) suggest to us that, besides the contribution of the Li_2MnO_3 impurity, they would be affected by the presence of paramagnetic Co^{2+} ions.

Electrical Conductivity. $LiMn_2O_4$ is an n-type semiconductor in which the electrical conductivity is due to electron hopping from the Mn^{3+} to the Mn^{4+} ion.[4,6,7] The grain interior dc conductivity of the *heated* samples is strongly affected by the cobalt−manganese substitution as shown in Figure 9, inset. In the spinel structure, the transition metal ions (TM) are placed in octahedral sites; each octahedron sharing edges with six octahedra. In this unit it is easy to see that if TM′ ions replace the TM ions, the former are only located in neighboring positions when their content is above 37.5%, i.e., when at least 1.5 of the 4 ions per unit are TM′ ions. It agrees with the sharp increase in conductivity observed at $y >$ 0.65, i.e., >32% of Co, and suggests a change in the electron hopping from manganese to cobalt. Furthermore, the Co ions must be at the same crystallographic site (16d) and in two oxidation states differing by unity.

(29) Aitchinson, P.; Ammundsen, B.; Jones, D. J.; Burns, G.; Roziére, J. *J. Mater. Chem.* **1999**, *9*, 3125.
(30) Zhecheva, E.; Stoyanova, R.; Gorova, M.; Lavela, P.; Tirado, J. L. *Solid State Ionics* **2001**, *140*, 19.
(31) Shannon, R. D. *Acta Crystallogr.* **1976**, *A32*, 751.

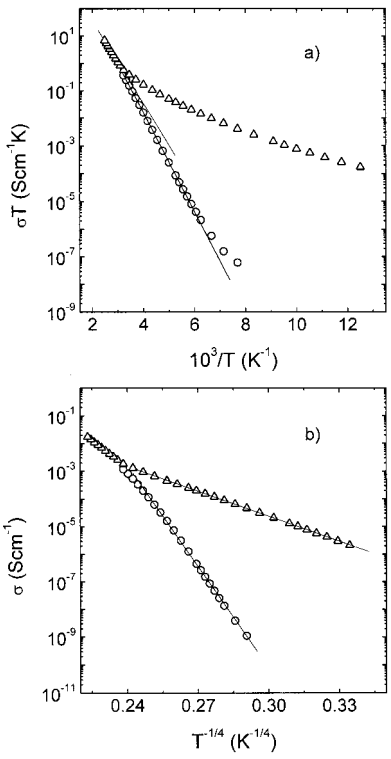

Figure 11. Plot of: σT vs 1000/T (a) and σ vs $T^{-1/4}$ (b). Circles and triangles stand for the *heated* samples at $y = 0.11$ and 1, respectively.

As the *heated* samples are reduced samples due to the net oxygen loss, it is plausible that some Co^{3+} ions are reduced to Co^{2+} ions. When all Co ions have the same oxidation state, electron hopping cannot occur. Thus, when the *heated* sample at $y = 0.85$ is oxidized by annealing (all Co is 3+), the conductivity found is close to that of the *heated* samples at $y < 0.65$; i.e., the conductivity is close to the one of the samples in which electron hopping occurs via Mn^{3+}/Mn^{4+} ions.

The conductivity (σT) vs reciprocal temperature (1000/T) for the *heated* samples at $y = 0.11$ and $y = 1$ are plotted in Figure 11a. At high temperatures a linear dependence is observed in agreement with the Mott model of phonon-assisted hopping of small polaron among transition metal ions in two-valence states,[32] i.e., either Mn^{3+} and Mn^{4+} or Co^{2+} and Co^{3+}. The experimental data are well fitted to the expression:

$$\sigma T = n_0[e^2C(1 - C)/k_BR] \exp(-2\alpha R) \exp(-W/k_BT) \quad (1)$$

where n_0 is the optical phonon frequency (n_0 was taken as 1×10^{12} s^{-1} because the phonon frequency is of the order of 1×10^{12} Hz), e is the charge of the electron, C is the $Mn^{3+}/(Mn^{3+} + Mn^{4+})$ and $Co^{2+}/(Co^{2+} + Co^{3+})$ ratios for the samples at $y \leq 0.65$ and $y > 0.65$, respectively, k_B is the Boltzmann constant, T is the temperature, R is either the Mn−Mn or Co−Co distance (as deduced from $R = a\sqrt{2}/4$, where a is the cubic lattice parameter), α^{-1} is the localization length of the s-like wave function which describes the localized state at each transition metal site, and W is the activation energy for hopping. The fitting parameters (W and α) obtained for all compositions are outlined in Table 1. W decreases continuously from 0.35 to 0.30 eV as y increases and its values are similar for electron hopping among Mn^{3+}/Mn^{4+} sites and Co^{2+}/Co^{3+} sites. The activation energies found are comparable to those reported for spinel-type compounds having Fe ions.[33] The values of α indicate a strong localization of the electrons at the manganese and cobalt sites.[34]

Table 1. Parameters Deduced from the Fit of the Conductivity of the *Heated* Samples According to the Nearest-Neighbor Hopping Model and the Variable Range Hopping Model

cobalt content (y)	C^a	R (Å)^b	W (eV)	α (Å^{-1})	$N(E_F)$ (eV^{-1} cm^{-3})
0.11	0.47	2.91	0.35	0.38	5.3×10^{19}
0.50	0.35	2.90	0.32	0.56	3.2×10^{20}
0.65	0.33	2.88	0.32	0.59	4.3×10^{20}
0.85	0.22	2.86	0.31	0.45	2.7×10^{22}
1.0	0.08	2.85	0.30	0.44	2.2×10^{22}

[a] $C = Mn^{3+}/(Mn^{3+} + Mn^{4+})$ for the samples at $y \leq 0.65$; $C = Co^{2+}/(Co^{2+} + Co^{3+})$ for the samples at $y > 0.65$. [b] $R = a\sqrt{2}/4$, where a is the cubic lattice parameter.

At low temperatures the experimental data of Figure 11a deviate systematically from the straight line. In this case. the temperature dependence of conductivity can be described by the variable-range-hopping model.[35] According to this model, electron hopping occurs preferentially beyond the nearest neighbor transition metal ions at different energies, these energies being lower than the energy required for hopping among nearest neighbor ions. The temperature dependence of the conductivity follows the expression:

$$\sigma = s_0 \exp[(-T_0/T)]^{1/4} \quad (2)$$

where s_0 is a constant and $T_0 = 19.44\alpha^3/k_BN(E_F)$; $N(E_F)$ is the density of states at the Fermi level. In Figure 11b, the linear dependence observed in the plot of σ vs $T^{-1/4}$ indicates that the experimental data are accounted for the variable range-hopping model. The calculated $N(E_F)$ for the different compositions is also listed in Table 1. It can be noted that for the samples at $y \leq 0.65$ $N(E_F)$ is nearly the same, but increases by 2 orders of magnitude for the samples at $y > 0.65$. This result justifies the sharp increase in conductivity already mentioned. The large value of $N(E_F)$ for the Co-rich samples may be explained by assuming that the states near the Fermi level are confined to a narrow energy band of nearly 0.1 eV.[36]

Electrochemical Behavior. The insertion of lithium into the Co-doped samples takes place in two steps at ca. 4 and 5 V, which correspond to the Mn^{4+}/Mn^{3+} and Co^{4+}/Co^{3+} reductions, respectively.[16,26,27] The amount of inserted lithium, Δx, at those voltages vs y for both the *as prepared* and *heated* samples is shown in Figure 12. For the *as prepared* samples, Δx_{4V} (open circles) decreases linearly as y increases and the experimental values are close to the expected ones (solid straight line). It confirms the substitution for Mn^{3+} by Co^{3+} in $LiMn_2O_4$. Only for $y = 0$ and 1 a deviation from the straight

(32) Mott, N. F.; *J. Non-Cryst. Solids* **1968**, *1*, 1.

(33) Smit, J.; Wijn, H. P. *Ferrites,* John Wiley and Sons: New York, 1959.
(34) Fine, M. E.; Chiou, C. *Phys. Rev.* **1957**, *105*, 121.
(35) Mott, N. F. *Philos. Mag.* **1969**, *19*, 835.
(36) Davis, E. A.; Mott, N. F. *Philos. Mag.* **1970**, *22*, 903.

Table 2. Composition and Chemical Formulas for the *As Prepared* and *Heated* Samples

as prepared $LiCo^{3+}_yMn^{3+}_{1-y}Mn^{4+}O_4$		heated $LiCo^{2+}_pCo^{3+}_{y-p}Mn^{3+}_{1-y+q}Mn^{4+}_{1-q}O_{4-\delta}$	
nominal	Mn^{3+}exptl[a]	δ[b]	chem formulas[c]
$LiMn^{3+}Mn^{4+}O_4$	0.84	0	
$LiCo^{3+}_{0.06}Mn^{3+}_{1.94}Mn^{4+}O_4$		0	
$LiCo^{3+}_{0.11}Mn^{3+}_{0.89}Mn^{4+}O_4$		0.01	
$LiCo^{3+}_{0.17}Mn^{3+}_{0.83}Mn^{4+}O_4$		0.01	
$LiCo^{3+}_{0.25}Mn^{3+}_{0.75}Mn^{4+}O_4$		0.01	
$LiCo^{3+}_{0.33}Mn^{3+}_{0.67}Mn^{4+}O_4$	0.61	0.03	$LiCo^{2+}_{0.14}Co^{3+}_{0.19}Mn^{3+}_{0.59}Mn^{4+}_{1.08}O_{3.97}$
$LiCo^{3+}_{0.5}Mn^{3+}_{0.5}Mn^{4+}O_4$	0.48	0.03	$LiCo^{2+}_{0.03}Co^{3+}_{0.47}Mn^{3+}_{0.53}Mn^{4+}_{0.97}O_{3.97}$
$LiCo^{3+}_{0.65}Mn^{3+}_{0.35}Mn^{4+}O_4$	0.31	0.11	$LiCo^{2+}_{0.12}Co^{3+}_{0.53}Mn^{3+}_{0.45}Mn^{4+}_{0.90}O_{3.89}$
$LiCo^{3+}_{0.75}Mn^{3+}_{0.25}Mn^{4+}O_4$		0.17	
$LiCo^{3+}_{0.8}Mn^{3+}_{0.2}Mn^{4+}O_4$	0.21	0.16	$LiCo^{2+}_{0.22}Co^{3+}_{0.58}Mn^{3+}_{0.30}Mn^{4+}_{0.90}O_{3.84}$
$LiCo^{3+}_{0.85}Mn^{3+}_{0.15}Mn^{4+}O_4$	0.11	0.17	$LiCo^{2+}_{0.19}Co^{3+}_{0.66}Mn^{3+}_{0.30}Mn^{4+}_{0.85}O_{3.83}$
$LiCo^{3+}Mn^{4+}O_4$	0.14	0.12	$LiCo^{2+}_{0.08}Co^{3+}_{0.92}Mn^{3+}_{0.16}Mn^{4+}_{0.84}O_{3.88}$

[a] From electrochemical measurements. [b] From TG analysis. [c] From TG and electrochemical measurements.

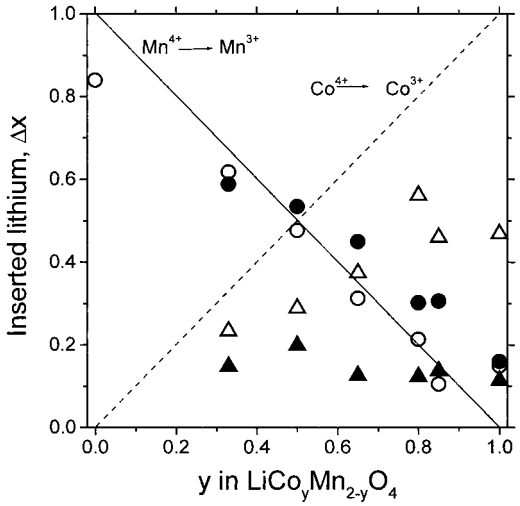

Figure 12. Inserted lithium (Δx) vs Co content (y) deduced from the first discharge curves. Open and solid circles stand for lithium inserted in the 4 V region for the *as prepared*, and *heated* samples, respectively. Open and solid triangles stand for lithium inserted in the 5 V region for the *as prepared* and *heated* samples, respectively. The solid and dotted straight lines correspond to the expected lithium insertion according to one Li^+ per Mn^{3+} and one Li^+ per Co^{3+}, respectively.

line is observed. In the former case, experimental values close to 0.8 Li^+ inserted per formula are usually reported.[37] In the latter case, the presence of a small plateau at 4 V (Figure 7a) indicates that some Mn^{3+} remains in the spinel. This fact, which is not well understood yet, has also been observed by other authors[15,16] and was accounted for by assuming a composition somewhat different from $LiCo^{3+}Mn^{4+}O_4$. In the 5 V region (open triangles), Δx_{5V} increases as y increases and reaches a maximum value for $y = 0.8$. In all cases, Δx_{5V} is lower than expected on the basis of one Li^+ inserted per Co^{3+} (dashed straight line). The difference between the experimental and the expected values is more important as y increases in agreement with results reported by other authors.[16,21] It seems that, contrary to Mn^{3+}, not all the Co^{3+} in the spinel is electrochemically active at the voltages examined.

For the *heated* samples, the lithium inserted at ca. 4 V (closed circles) and 5 V (closed triangles) is shown in Figure 12. We observe that Δx_{4V} is higher for the *heated* samples than for the *as prepared* ones evidencing more Mn^{3+} in the former than in the latter. In the 5 V region, Δx_{5V} shows a value close to 0.12 for all compositions indicating less electrochemically active Co^{3+} compared to the *as prepared* samples. Therefore, the thermal treatment performed to obtain the *heated* samples produces an increase in the amount of Mn^{3+} and a decrease in the amount of Co^{3+} because of the reduction of some Mn^{4+} to Mn^{3+} and some Co^{3+} to Co^{2+}.

Chemical Composition. Having in mind that the *heated* samples are obtained from heating/cooling treatment of the *as prepared* samples and that in this process there is (i) a net oxygen loss and (ii) a reduction of some Mn^{4+} and Co^{3+}, the reaction can be expressed as follows

$$LiCo^{3+}_yMn^{3+}_{1-y}Mn^{4+}O_4 \rightarrow LiCo^{2+}_pCo^{3+}_{y-p}Mn^{3+}_{1-y+q}Mn^{4+}_{1-q}O_{4-\delta} + \delta/2O_2\uparrow \quad (3)$$

where the subscripts p and q stand for the Co^{2+} and Mn^{3+} formed in this reaction. From the balance of charges in the *heated* samples, it is easy to see that $p + q = 2\delta$. Since the δ and q values are accurately determined from the TG and electrochemical experiments, respectively, the p values can be calculated. The chemical formulas deduced for the *heated* samples are outlined in Table 2. In this table, the chemical formulas of the *as prepared* samples are included as references.

Conclusions

High-temperature $LiCo_yMn_{2-y}O_{4-\delta}$ ($0.3 \le y \le 1$, $0.03 \le \delta \le 0.17$) compounds with cubic spinel structure have been prepared. They are oxygen-deficient phases in which Mn^{4+} and Co^{3+} are partially reduced to Mn^{3+} and Co^{2+}, respectively. The electrical conductivity depends on the Co content and increases sharply for $y > 0.65$. A change in electron hopping from Mn^{3+}/Mn^{4+} to Co^{2+}/Co^{3+} has been found. The discharge capacity measured at ca. 4 V is higher than at ca. 5 V over the whole compositional range examined.

Acknowledgment. Financial support by CICyT (Project MAT 98-0904) and CAM (Project 07*N*/0059/1998) is gratefully acknowledged. S.M. thanks the Spanish Education and Culture Ministry for a fellowship.

CM011219V

(37) Linder, D., Ed. *Handbook of batteries*, 8th ed.; McGraw-Hill, New York, 1995.

(38) During the final revision of this manuscript, a letter by Reeves et al. (Reeves, N.; Kirk, A.; West, A. R. *J. Mater. Chem.* **2001**, *11*, 249) about the thermal treatment of $LiCoMnO_4$ has appeared.